Supporting Information for

"Duplicating Plasmonic Hotspots by Matched Nanoantenna Pairs for Remote Nanogap Enhanced Spectroscopy"

Yang Li,[†] Huatian Hu,[‡] Wei Jiang,[†] Junjun Shi,[‡] Naomi J. Halas,[§] Peter Nordlander,[§] Shunping Zhang,*[,†] and Hongxing Xu*[,†,‡]

[†]School of Physics and Technology, Center for Nanoscience and Nanotechnology, and Key Laboratory of Artificial Micro- and Nanostructures of Ministry of Education, Wuhan University, Wuhan 430072, China.

[‡]The Institute for Advanced Studies, Wuhan University, Wuhan 430072, China.

[§]Department of Physics and Astronomy, Department of Electrical and Computer Engineering and Laboratory for Nanophotonics, Rice University, Houston, Texas 77005, United States.

Corresponding Author

*E-mail: spzhang@whu.edu.cn. Phone: +8627 68752219.

*E-mail: hxxu@whu.edu.cn. Phone: +8627 68752253.

S1. Magnetic field distributions of the cavity plasmon modes in the structures

In the main text Fig. 1, we have presented the numerical simulations for the electric field properties of the silver nanowire (Ag NW) on the gold mirror (NWOM) and the silver nanocubes (Ag NCs) on a gold mirror (NCOM). To reveal the unique magnetic properties of the Ag NW and Ag NC on a gold film, we also present the magnetic field distributions (Fig. S1) of the cavity plasmon modes with the same geometry. A 96 nm Ag NC and an 86 nm Ag NW are deposited on a 3 nm ALD-covered Au film to form the NCOM and NWOM structures. Both covered by 3 nm PVP, the Ag NC has a 23 nm curvature on the edges and corners while the Ag NW has a 5 nm curvature around the corners. On top of the structures, we grow a 5 nm ALD layer as the protection against oxidization/sulfonation. Full-wave simulations are performed in a 3D model for the NCOM and a 2D model for the NWOM. The dielectric function of the silver and gold are taken from the measured data by Johnson & Christy[1]. The distributions of the magnetic field $|\mathbf{H}|/|\mathbf{H_0}|$ of the two geometries are given in Fig. S1(a) and (b), with the resonance peaks around 765 nm and 810 nm, respectively. In these structures, the charge distribution can form a current loop in the nanogap[2], and inducing a substantial magnetic field enhancement.

The magnetic field $\mathbf{H}_y$ of the SPPs on the substrate is shown in Figure S1(c), where the SPPs propagated symmetrically and bi-directionally on the gold film under excitation at the center of the Ag NW. The electric field $\mathbf{E}_z$ will be discussed in Fig. S2.

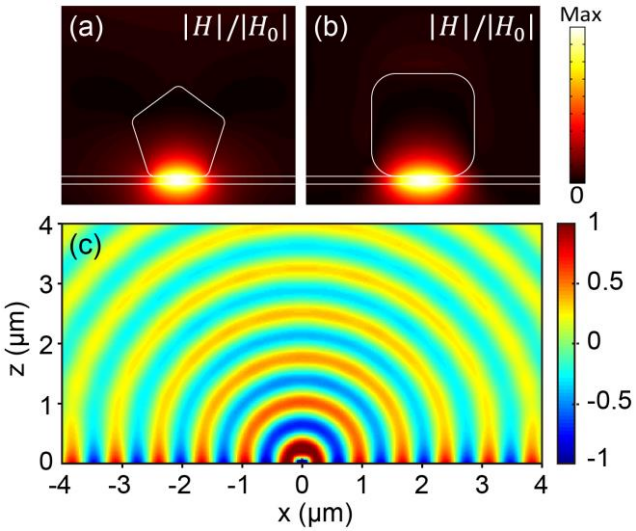

Figure S1. Modes analysis of an 86 nm-diameter Ag NW and 96 nm Ag NC on a gold film with a 3 nm Al_2O_3 spacer and 5 nm Al_2O_3 protective coating. (a) and (b) are the corresponding magnetic field distributions of the cavity plasmon modes in the Ag NW and Ag NC on a gold film. (c) The distribution of the normalized magnetic field $\mathbf{H}_y$ of the SPPs launched from the Ag NW on a gold film under a Gaussian beam excitation at the center of the Ag NW.

S2. The SPPs launched from the Ag NW on a gold film

Effective excitation and delivery of the SPPs is a critical factor for our device. Here the NWOM structure acts as a receiving antenna to convert free space photons into localized nanocavity plasmon modes. Analogous to the photons escaping through the Fabry–Pérot cavity, in the subwavelength regime, the SPPs can leak from the nanocavity without significant momentum mismatch.

The NWOM structure is illuminated by a Gaussian beam (1 μm beam waist diameter) along the z-axis to excite the SPPs. The excitation wavelength is 765 nm, which exactly matches the resonance wavelength of the NWOM system (The same geometry as Fig. 1 in the main text). We can clearly observe that the SPPs propagate in two different directions. In Fig. S2(a), when the incident Gaussian beam is concentrically focused on the Ag NW, the magnetic dipoles are located at the center of the NW. The ratio of the SPPs propagate in the negative and positive parts of the x-axis is the same. The SPPs propagate on the interface symmetrically and bi-directionally. While under the off-centered excitation, due to the broken symmetry, and the elliptically polarized magnetic dipoles can be excited. As shown in Fig. S2(b) and (c), the SPPs are observed to propagate asymmetrically in the simulations. When the Gaussian beam illuminates at the left side of the Ag NW ($x < 0$), the SPPs propagate preferentially to the positive part of the x-axis, and *vice versa*. Further, we simulated the power flow streamline modulated by the NWOM under the excitation of a Gaussian beam in section S3.

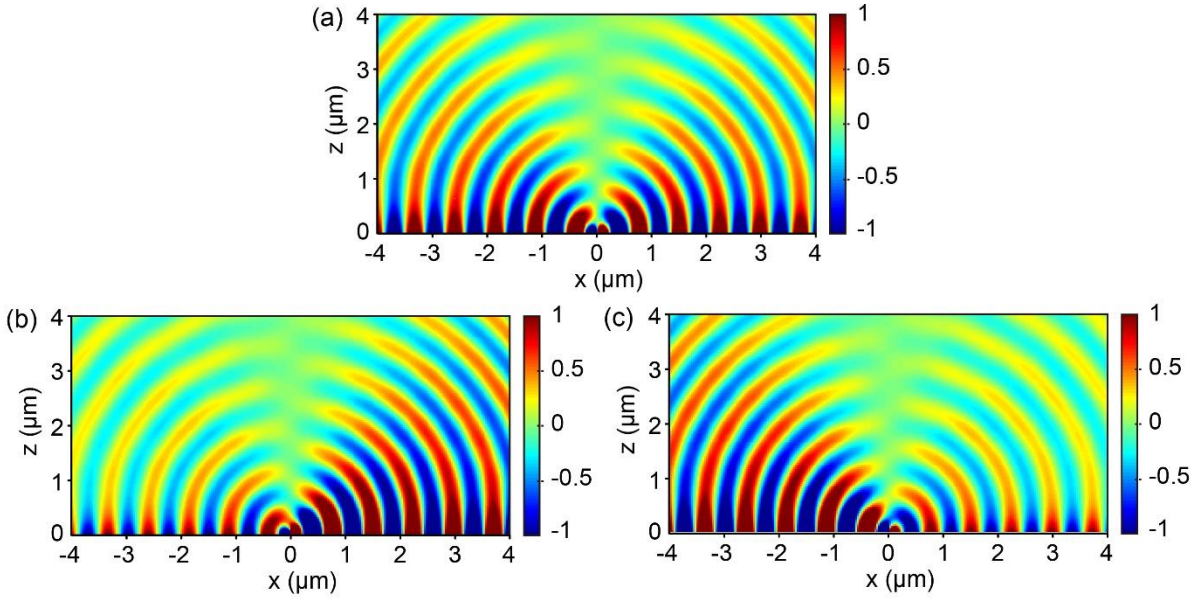

Figure S2. The distribution of the scattered $\mathbf{E}_z$ component of the SPPs launched from the Ag NW on a gold film under excitation (a) at the center of the Ag NW, (b) at the left part of the Ag NW and (c) at the right part of the Ag NW.

In addition, in Figure S3, we prove that the SPPs field has a mostly vertical electric field due to the equipotentiality of the metal. Thus, the cavity plasmon modes of the NCOM can be most effectively excited by this vertical E-field.

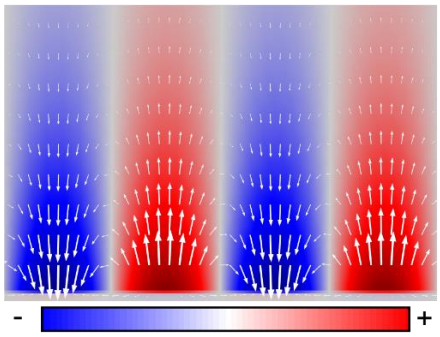

Figure S3. The electric field of the SPPs propagating along a gold surface has a major vertical component. The white arrows are the electric field vectors.

S3. The power flow streamline modulated by NWOM under the excitation of Gaussian beam

A linearly polarized Gaussian beam, which can be viewed as the superposition of two opposite circularly-polarized beams, initially holds no angular momentum. When it interacts with the NWOM, we observe an intense curvature of the energy flow due to spin-orbit interaction[3] (Fig. S4(b)-(d)), which is finally absorbed by the structure. When the Gaussian beam is concentrically illuminating the structure (Fig. S4(b)), we observe symmetric curvatures on both sides, which gives no extra angular momentum. As the SPPs propagating towards different sides have opposite angular momentums, concentric illumination will give rise to symmetric SPPs excitation.

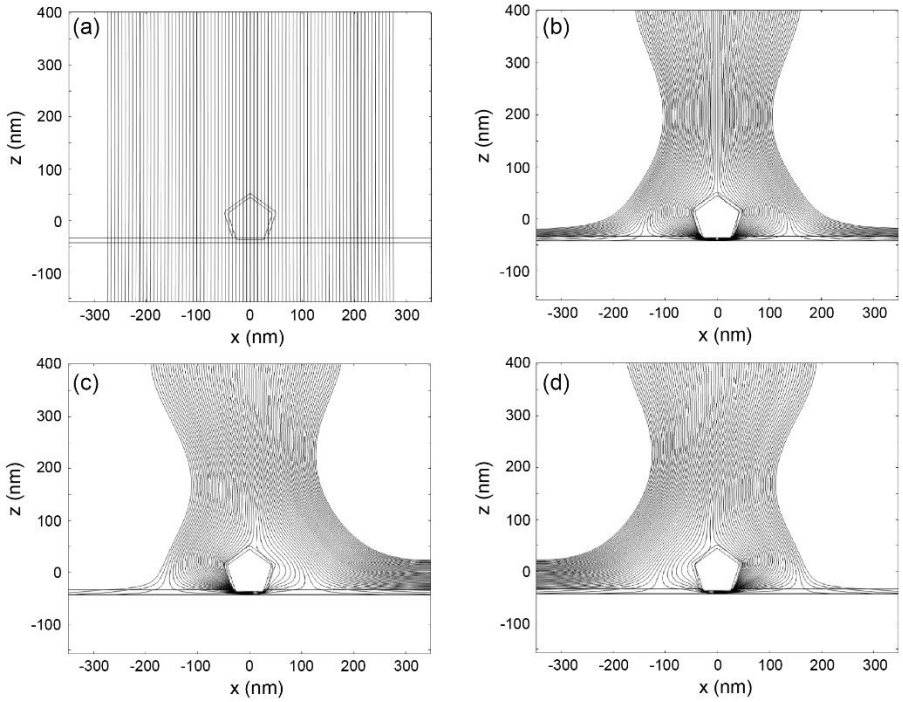

Figure S4. (a) The power flow streamlines of a background Gaussian beam without the modulation of the NWOM structure. (b-d) the power flow modulated by the NWOM with Δx = 0 nm, +500 nm, -500 nm.

However, when the Gaussian beam is illuminating eccentrically, Fig. S4(c) (Δx = +500 nm), for instance, we observe a huge curvature of Poynting vectors on the left side and a slight curvature on the right side. When these beams are absorbed by the structure, the angular momentum should be conserved by emitting SPPs with specific angular momentums difference. It is well-known that the spin angular momentum of SPPs is determined by $\mathbf{k}\times\boldsymbol{\eta}$ ($\mathbf{k}$ is the wave vector of SPPs and the $\boldsymbol{\eta}$ is the decay)[4]. It is safe to claim that the Δx = +500 nm eccentric illumination will effectively excite more SPPs in the positive x-direction due to the conservation of angular momentum. The orbital angular momentum of the near-field light transforms into the spin angular momentum of the SPPs. Likewise, the Δx = -500 nm eccentric illumination in Fig. S4(d) will give the opposite results according to the same mechanism.

S4. The calculation of coupling efficiency of Ag NW on a gold mirror system

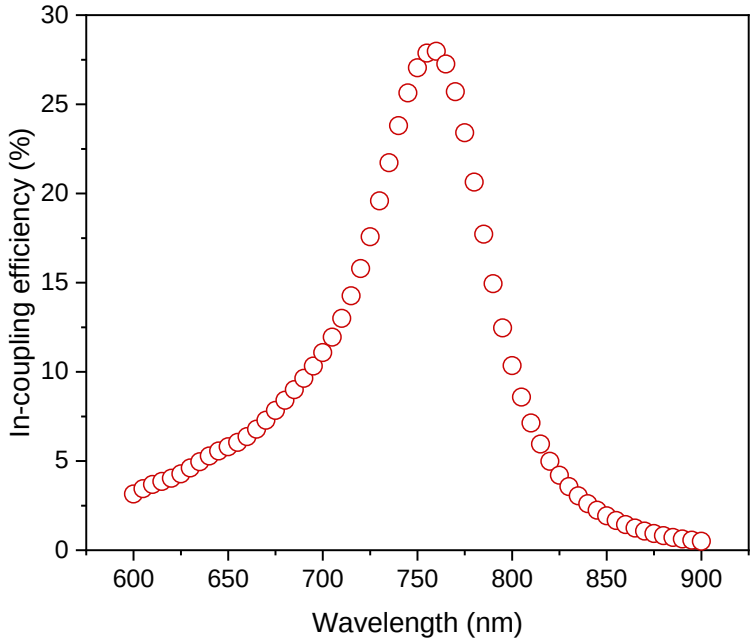

Figure S5. The in-coupling efficiency of the conversion from light to SPPs, against the excitation wavelength for a NWOM structure.

The coupling efficiency of free-space photons into SPP modes is a crucial parameter for various plasmonic nanostructures. Especially in plasmonic waveguides, the coupling efficiency directly determines the total propagation distance of SPPs. As for our metal-insulator-metal nanocavity supporting huge electric/magnetic field enhancement, high coupling efficiency and a large extinction cross-section are expected.

The coupling efficiency of free-space photons into SPPs via a NWOM system is calculated by the far-field transformation, which distinguishes the free-space radiation from the guided-mode based on reciprocity theory using an open-source package[5]. A 2D NWOM model was established and a transformation surface was created to surround all the inhomogeneities, and the equivalence principle[6] can be applied to investigate the far-field diagram. Green's function of stratified substrates and claddings is needed to predict the far-field radiation from the equivalent currents on the transformation surface. Yet the analytical solution of that Green's

function is hard to obtain. Thus, the reciprocity method[5, 6] is utilized, and the modes created by the equivalent sources are predicted by inversely using test modes to excite the field at the sources.

For an NWOM structure with an 86 nm Ag NW, under the excitation of an experimentally focused Gaussian beam with a waist diameter approaching the diffraction limit, the coupling efficiency approaches the maximum of 28% on resonance (also see Fig. S9 for beam waist dependency). While for a 1 um beam waist diameter, the coupling efficiency is around 25.8%. This coupling efficiency is surprisingly high for a single nanostructure with such a small geometrical size. Meanwhile, such a high coupling efficiency guarantees a sufficient propagation distance of SPPs, which lays a foundation for remote SERS detection. Also, the excited SPPs can cover large areas on both sides of the Ag NW, depending on the size of the beam spot, which is an ideal SPPs source for complex large-area on-chip plasmonic structures.

S5. The remote SERS enhancement in the excitation-collection separated plasmonic nanoantenna pairs

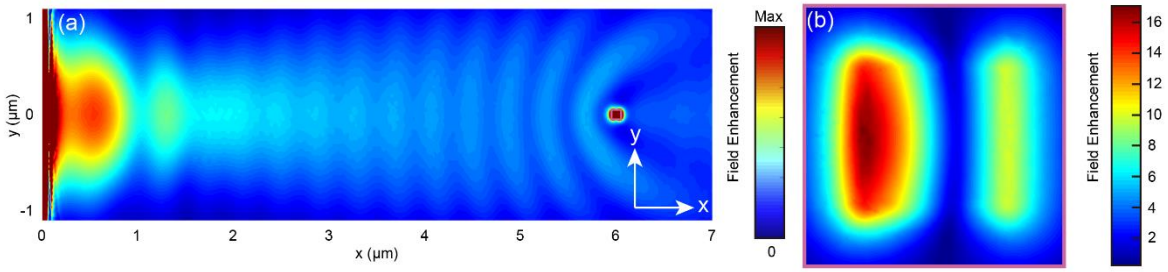

Figure S6. Calculation of electromagnetic field enhancement in the NWOM-NCOM system. (a) The E-field along the direction perpendicular to the Ag NW with the local excitation on the Ag NW. (b) The E-field enhancement in the NCOM configuration, which corresponds to the area in the pink box in (a).

In order to understand and evaluate the effect of such a matched nanoantenna pair on remote excitation Raman spectroscopy, corresponding theoretical simulations were performed. For the sake of simplicity, we set the model as a matched NWOM-NCOM system, where the Ag NW and Ag NC were on an ultra-smooth gold film separated by 3 nm ALD spacer, and the single NC were located 6 μm away from the Ag NW. The NWOM structure was illuminated by a Gaussian beam (1 μm waist diameter) along the z-axis to excite the SPPs, and then we can obtain the local field enhancement of the NCOM structure. As shown in Fig. S6(b), the maximum electric field enhancement at the NCOM area is around 17, which is of the same order of magnitude as reported in ref [7]. While in our geometry, Raman signals can be triggered on tens of transmitting nanoantennas, which would extraordinarily boost the total detection efficiency.

S6. The details of the sample for remote SERS detection

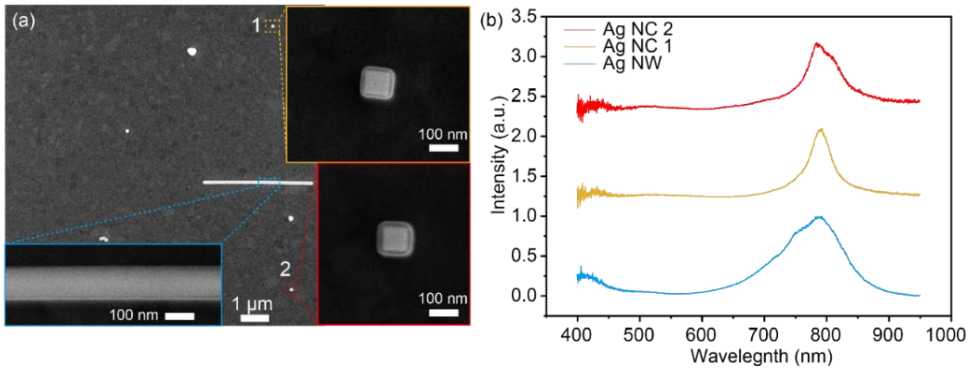

Figure S7. (a) The SEM image of the NWOM-NCOM sample for remote SERS detection. Insets are the corresponding SEM images of the Ag NCs and the Ag NW. (b) The dark field scattering spectrums of the target Ag NW and Ag NCs in (a).

In Fig. S7(a), we show the SEM image of the NWOM-NCOM sample for remote SERS detection. The geometrical parameters of the corresponding Ag NW and Ag NCs can be found in the insets. Also, we performed the dark-field scattering spectrums of the target Ag NW and Ag NCs in Fig. S7(b). It is clear that all of them resonate at the wavelength around 785 nm, which matches perfectly with the excitation wavelength.

S7. The Discussion of the factors that affect the in-coupling efficiency

(1) Size-dependence. If the wavelength of the laser is fixed, the optimized parameters are the set that could create a resonant geometry in accordance with the excitation wavelength. Therefore, in this case, the change of the geometric parameter would shift the resonance and decrease the coupling efficiency. For an instant, we fix the Gaussian beam at 760 nm and change the nanowire diameter d_1 from 60 nm to 120 nm. Due to the detuning, as shown in Fig. S8a, the efficiency has a maximum when the $d_1 \sim 86$ nm.

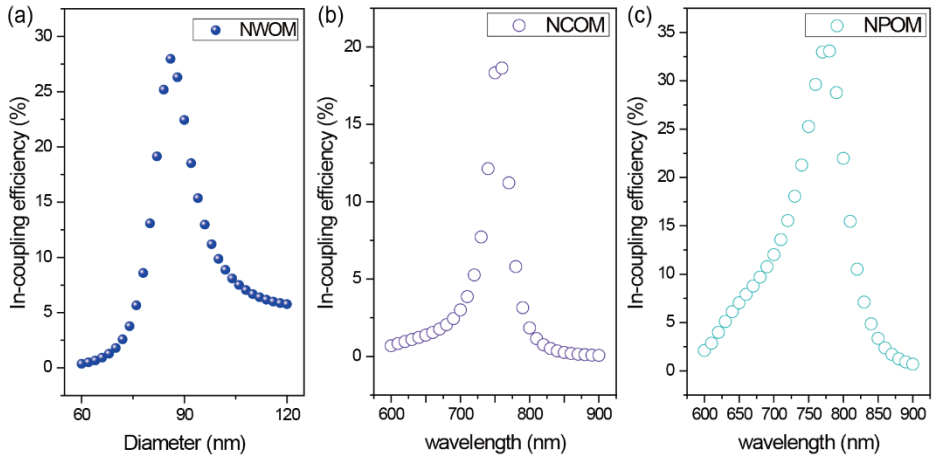

Figure S8. Factors that affect the in-coupling efficiency. (a) in-coupling efficiency versus the diameter of the Ag NW. Dependencies on the cross-section shapes, *e.g.* (b) NCOM and (c) NPOM.

(2) Shape-dependence. The in-coupling efficiency of the receiving antenna is one key parameter to drive the transmitting nanoantennas. We studied three typical structures (NWOM, NCOM, NPOM) to compare their coupling efficiencies. For fairness, we only replace the nanoparticle and leave the other geometrical parameters (spacer, PVP, coating, etc.) and the Gaussian excitation the same. Moreover, we tune the resonances to be roughly the same by modifying the diameter of the nanoparticles.

As shown in Fig. S5, the 3 nm PVP covered Ag NW on the Au-film has the maximum coupling efficiency of 28%. An 88.5 nm silver nanocube covered by 3 nm PVP is placed on the Au-film, we find the maximum coupling efficiency around 19% on resonance ~ 760 nm (Figure S8(b)). While for a 150 nm silver nanosphere with 48 nm bottom facet covered by 3 nm PVP on the Au-film, the maximum coupling efficiency is around 33% on resonance ~780 nm (Figure S8(c)).

(3) Laser spot-dependence. In general, increasing the spatial overlap between the incident light and the Ag NW can improve the in-coupling efficiency. Therefore, the size of the excitation laser spot has a great impact on the in-coupling efficiency. Here we calculated the relationship between the beam waist diameter and the in-coupling efficiency, which shows that the in-coupling efficiency approaches to it limit ~ 28%. This value is already the maximum by focusing the laser spot towards a diffraction-limited size. To further improve the in-coupling efficiency, it may be necessary to increase the diameter of the Ag NW.

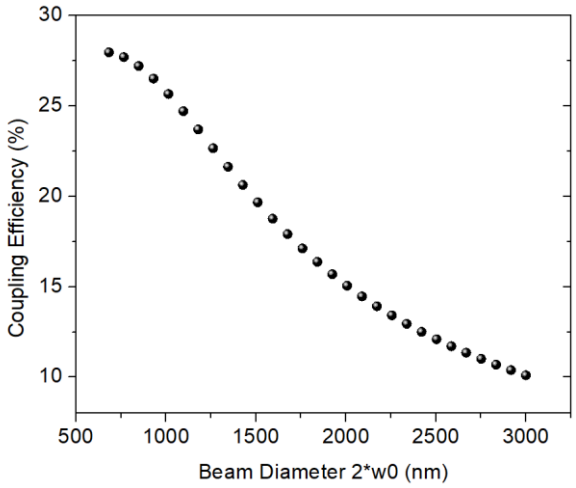

Figure S9. The dependence of in-coupling efficiency on the laser spot diameter.

S8. The out-coupling from the transmitting nanoantennas

(1) Distance dependent out-coupling. The receiving and transmitting antennas are bridged by the SPPs on the metal-insulator interface which experiences an exponential decay. Thus, the distance between the Ag NW and Ag NC directly determines the out-coupling power for the transmitting antenna (NCOM).

To reveal the distance-dependent out-coupling, firstly, we theoretically study the SPPs propagating length, which would explain the relationship between the out-coupling intensity and the distance between receiving and transmitting nanoantennas. We use the boundary mode analysis to study the air- Al_2O_3-Au layers and calculate the propagation length of the SPPs L_{SPP}

in Fig. S10.

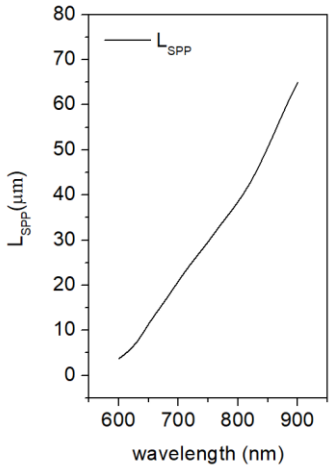

Figure S10. The propagation length of the SPPs in the configuration of the air-Al_2O_3-Au multilayer.

Therefore, the far-field emission power (P_{FF}) from the Ag NC, x_0 away from the Ag NW, should be $P_{FF} = P_0 e^{-x_0/L_{SPP}} \cdot \eta_{out}$, where the P_0 is the power of SPPs in-coupled by the Ag NW and the η_{out} is the out-coupling efficiency of the transmitting antenna (Ag NC). In conclusion, the total outcoupling intensity of the transmitting antenna would show an exponential decay according to the distance away from the receiving antenna.

(2) Orientation independent out-coupling. These calculations suggest that the out-coupling radiation is not orientation-dependent. In the FEM simulation, we use the boundary mode analysis to set the SPPs as the excitation for this NCOM configuration (mimicking the excitation by the SPPs launched by the NWOM). The far-field scattering from the nanocubes with different orientations θ ranging from 0° to 90° are demonstrated, which shows the same scattering intensity. Due to the 4 fold symmetry, 90° to 360° data have been included in the present calculation.

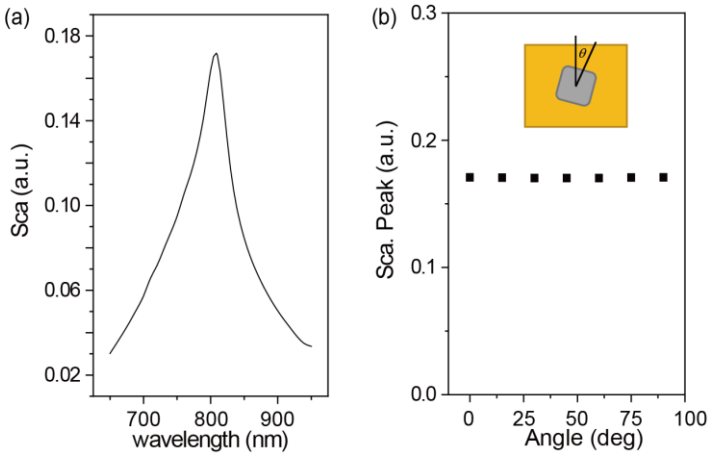

Figure S11. (a) The scattering of the NCOM system. (b) The peak intensity of the NCOM with different orientations.

(3) The out-coupling efficiency from different configurations. The out-coupling efficiency is a significant factor in the system. Here we use SPPs to excite three commonly

used configurations (NWOM, NCOM and NPOM) to calculate the scattering coefficient (Q_{sca} = P_{sca}/ P_{SPP}). The results are shown in the Figure S12, where the NCOM system shows the best Q_{sca}, corresponding to the best outcoupling efficiency.

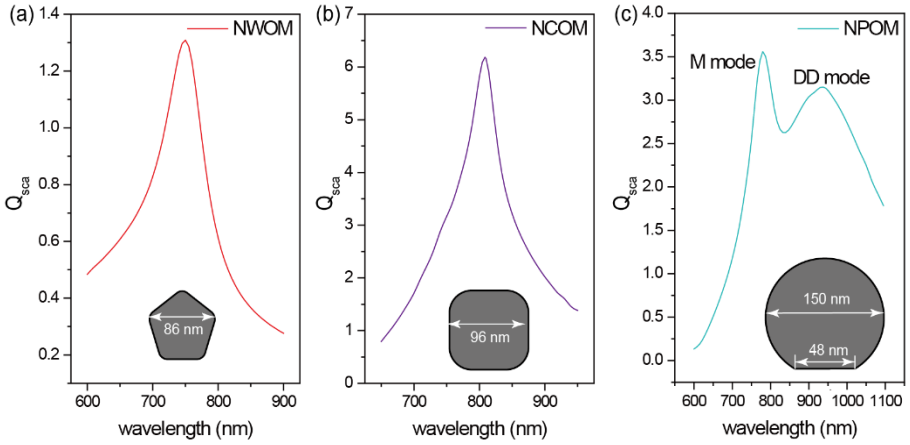

Figure S12. The scattering coefficients of nanowire on mirror (NWOM), nanocube on mirror (NCOM) and nanoparticle on mirror (NPOM) configurations.

S9. Quantify the Raman signal-to-noise ratios in the two excitation methods.

As shown in Fig. S13, we marked out the Raman signal and the background noise and obtained the signal-to-noise ratio, SNR= S_{signal}/S_{noise}. Then we quantitatively calculated the signal-to-noise ratio (SNR) of the four characteristic Raman peaks from NC1 and NC2 (as shown in main text Fig. 5) under two excitation methods, the results are shown in Table 1.

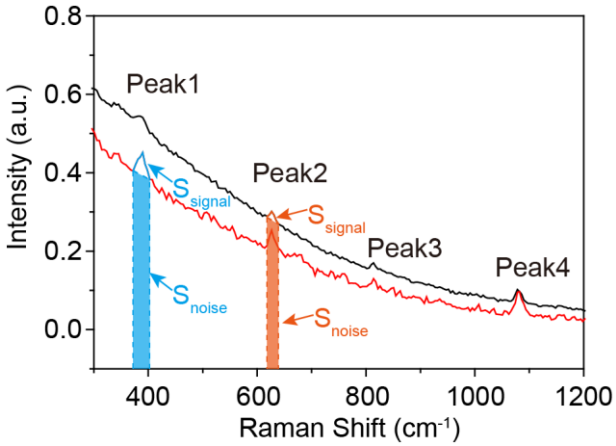

Figure S13. The remote and direct excitation Raman spectra from NC2 in the main text, Fig. 5(d).

Table 1. Quantify the Raman signal-to-noise ratios in the two excitation methods.

SNR= S_{signal}/S_{noise}		Peak1	Peak2	Peak3	Peak4
NC1	Remote NP1	0.13	0.136	0.181	0.662
	Local NP1	0.072	0.171	0.166	0.876
NC2	Remote NP2	0.077	0.092	0.105	0.678
	Local NP2	0.025	0.025	0.044	0.205

References

(1) Johnson, P. B.; Christy, R. W. Optical Constants of the Noble Metals. *Phys. Rev. B* 1972, 6, 4370-4379.

(2) Lassiter, J. B.; McGuire, F.; Mock, J. J.; Ciracì, C.; Hill, R. T.; Wiley, B. J.; Chilkoti, A.; Smith, D. R. Plasmonic Waveguide Modes of Film-Coupled Metallic Nanocubes. *Nano Lett.* 2013, 13, 5866-5872.

(3) Pan, D.; Wei, H.; Gao, L.; Xu, H. Strong Spin-Orbit Interaction of Light in Plasmonic Nanostructures and Nanocircuits. *Phys. Rev. Lett.* 2016, 117, 166803.

(4) Bliokh, K. Y.; Rodríguez-Fortuño, F. J.; Nori, F.; Zayats, A. V. Spin–Orbit Interactions of Light. *Nat. Photonics* 2015, 9, 796-808.

(5) Yang, J.; Hugonin, J.-P.; Lalanne, P. Near-to-Far Field Transformations for Radiative and Guided Waves. *ACS Photonics* 2016, 3, 395-402.

(6) Demarest, K.; Huang, Z.; Plumb, R. An Fdtd near- to Far-Zone Transformation for Scatterers Buried in Stratified Grounds. *IEEE Trans. Antennas Propag.* 1996, 44, 1150-1157.

(7) Fang, Y.; Wei, H.; Hao, F.; Nordlander, P.; Xu, H. Remote-Excitation Surface-Enhanced Raman Scattering Using Propagating Ag Nanowire Plasmons. *Nano Lett.* 2009, 9, 2049-53.